

Regional and Local Ionospheric Models Based on Millstone Hill Incoherent Scatter Radar Data

John M. Holt, Shun-Rong Zhang, and Michael J. Buonsanto ¹

Haystack Observatory, Massachusetts Institute of Technology, Westford, Massachusetts

Abstract. Local and regional statistical models to describe Millstone Hill incoherent scatter radar observations of electron density, electron temperature and ion temperature since 1976 are developed using a bin-fit technique. The local models generate ionospheric variations with local time, day number, and altitude from 150-1000 km. The prior day's F107 and the Ap index from the previous 3 hour period are keyed inputs to specify solar and geomagnetic activity. The regional models have a latitude coverage of 32-55° geodetic and an altitude coverage of 200-600 km. These climatology models are capable of reproducing primary ionospheric variation features seen in previous studies as well as several newly revealed features, such as the semiannual variation of electron density. They are accessible through the World Wide Web at the URL <http://www.openmadrival.org>.

1. Introduction

Given that global models may smear out features which are unique to a particular region, regional and local models can be very useful. Millstone Hill (42.6°N, 288.5°E, Apex magnetic latitude 54°) is a unique mid-latitude region in Eastern North America, and a region of critical importance for the United States National Space Weather Program (NSWP). At an L value of 3 it lies near the plasmopause boundary and may be considered "subauroral" during geomagnetically disturbed conditions. In this region the fact that the geomagnetic latitude is about 12° higher than the corresponding geographic latitude may cause high conductivities,

and thermospheric circulations over this near-magnetic pole site may lead to interesting annual/semiannual ionospheric variations [Rishbeth, 1998; Rishbeth et al., 2000]. Since the 1960s, incoherent scatter (IS) measurements of electron density N_e , electron temperature T_e , ion temperature T_i , and line-of-sight ion drifts have been acquired over Millstone Hill. The favorable location at subauroral latitudes combined with the great operational range afforded by the radar's steerable antenna permit observations over a latitude span encompassing the region between the polar cap and the near-equatorial ionosphere.

From the extensive database of Millstone Hill IS observations, empirical models of basic and derived IS parameters, including N_e , T_e , T_i , electric fields and parallel drifts, are being developed. Here we present results for the three scalar parameters. These models are very important in validating theoretical models and empirical global models such as International Reference Ionosphere (IRI) [Bilitza, 2000], and also they can be applied to addressing outstanding scientific issues related to the ionosphere and thermosphere climatology: e.g., the annual and solar cycle variations of N_e , the ionospheric trough, the so-called dusk effect, the dependence of T_e and T_i on magnetic activity, etc. In this paper, the data used cover the 25-year period from February 1976 to August 2001, over a 200-600 km height range and a 32-55° geodetic latitude span for regional modeling, and over a 150-1000 km height range and 39-45° latitude span for the higher-resolution local modeling. Most of measurements used in the regional model were within a few degrees of Millstone Hill's longitude, though at high altitudes some were as much as 25° to the west. At 1000 km, the data used in the local model can be up to 7° to the east or west of Millstone. We employ a bin fit technology to sort the data and construct models. This will be described, and then we discuss the distribution of the sorted data bins. Next, we give general descriptions of the main features of our model results. Finally, we summarize this work and provide information on model availability.

2. Data and Method

The Millstone Hill UHF IS radar system operates with a zenith-directed 68 m diameter fixed parabolic antenna, which commenced operation in 1963, and a fully-steerable 46 m antenna, which commenced operation in 1978. The electron density and plasma temperatures are determined from the received power and spectrum. Experiments are carried out for more than 1000 hours per year. Data are archived in the Millstone Hill Madri-

gal online database system, which contains an extensive body of ground-based measurements and models of the Earth's upper atmosphere and ionosphere. Altogether, 907 experiments were included in the models.

The statistical models are computed using a bin-fit technique, which combines data binning with least squares fitting. The measured N_e , T_e and T_i are separated into bins according to local time, altitude, and the day of year (to represent seasonal variations), and also to geodetic latitude for regional modeling. The bin size is 1 hour for local time and 61 days for the seasonal variation. For the regional model, the bin size is 1° from 32 - 55° geographic latitude, and 50 km from 200-600 km. For the local model, there are 12 altitude bins centered at 150, 175, 200, 225, 250, 300, 350, 400, 500, 600, 800, and 1000 km, and data are limited to 39 - 45° geodetic latitude. In each bin, the dependencies on solar and magnetic activity are determined through a sequential least squares fit based on Givens transforms [Gentleman, 1973] to the following equation:

$$P = \beta_0 + \beta_1 \times f + \beta_2 \times a + \beta_3 \times f \times a$$

where P is either N_e , T_e or T_i , the β s are fitting coefficients, and $f = (F107 - 135)/135$ and $a = (A_p - 15)/15$ are the normalized F107 and A_p indices. F107 is the previous day's 10.7 cm solar flux index, and A_p is the 3-hourly equivalent range index A_p for the previous 3 hours. Deviations of actual data from the model represent the remaining day-to-day variability due to such causes as tidal forcings, gravity waves, uncertainties in the solar EUV flux and high latitude forcings which are difficult to accurately specify. While the physics involved in ionospheric responses to F107 and A_p is rather complicated, we opt for the linear approximation for simplification while giving the correct general trends of variations for our climatology models. A separate study demonstrating detailed variation trends of the data with F107 and A_p indicates the general validity of our linear approximation in the fit formula.

3. Data distribution

The data distributions of the electron density and plasma temperatures are essentially the same. Therefore we discuss only the N_e data. For local modeling, the data density is very high in the 250-500 km range, at about 70-100 counts/km for a given day number and local time bin, corresponding to, for example, about 3000-7000 data points for the 300 km bin. For lower or higher altitudes, the number of data points is on the

order of 1000 for daytime and 500 for nighttime. More data were obtained in the January to April and September to October periods than in other months. For the regional models, more than 350 data points are present during the day, and 200 during the night in the latitude range 38-50° as shown in Figure 1. Most data are from periods of low magnetic activity, with $A_p < 20$, and there are also many data for $20 < A_p < 40$.

Figure 1

4. Result

Our local models reproduce the occurrence and evolution of a few interesting midlatitude ionospheric phenomena, including the well-known “seasonal anomaly” where the midday N_e is higher in winter than in summer and the morning N_e increases more steeply in winter [Rishbeth and Setty, 1961] due to the O/N₂ effect, the midday density depression (“bite-out”) which relates to the northward neutral wind drag [Kohl and King, 1967], the evening density peak in summer [Evans, 1965] (see the left panel of Figure 2), the “predawn effect” in the electron temperature T_e [Carlson, 1966], T_e enhancements in the morning and in the afternoon [Brace and Theis, 1981], and the unusual high T_e on winter nights [Evans, 1973]. There appears a striking feature that has not previously been reported for Millstone Hill in a statistical manner: the semiannual variation of N_e , most pronounced above the F_2 peak, as shown in the center panel of Figure 2. During the day, N_e increases from winter, reaching an maximum in spring, then decreases toward summer when it reaches an minimum; a similar pattern follows in the second half of the year. Relative to other midlatitude sites where semiannual variations occur [Balan et al., 1999], Millstone Hill is nearer the north geomagnetic pole, and the winter density is supposed, by the well-established thermospheric circulation theory [Rishbeth et al., 2000], to be highest, exceeding the equinox density when the zenith angle effect is less important. This semiannual feature needs to be further investigated.

Figure 2

Figure 2

As for the solar activity dependence, N_e and T_i generally increase with F107, but the N_e increase becomes smaller for very large F107 in winter during noon and later [Balan et al., 1994]. Figure 2 (the right panel) shows an example of electron density responses to the F107 change. T_e responses are more complicated depending on local time, season and altitude [see also Bilitza and Hoegy, 1990]. It generally increases with F107, but decreases in summer when N_e is not very high. With increasing geomagnetic activity, N_e is typically reduced in summer and equinox periods (negative storm), T_e is elevated during the night, and T_i is ele-

Figure 2

vated during almost the entire day.

The midlatitude ionospheric trough is often seen in Millstone Hill radar data [Holt *et al.*, 1983]. This feature is clearly seen in the regional N_e model (Figure 3) for high magnetic activity. The trough is basically an afternoon and nighttime feature, though it may also appear during the day [Evans *et al.*, 1983; Vo and Foster, 2001]. This ionospheric main trough is considered to be caused by plasma convection through the night-side in the absence of ionisation sources and O^+ chemical recombination in the presence of large electric fields [Rodger *et al.*, 1992; Foster, 1993]. Detailed discussions of the trough structure seen near Millstone Hill have recently been given by Vo and Foster [2001]. Associated with the density depression in the trough, T_e is found to be high due to the reduced cooling rate. Compared with IRI-95, the seasonally averaged N_e above Millstone Hill is lower. Also significantly different from the IRI is the occurrence of a T_e morning enhancement in winter: it peaks sharply near 0800 LT, while it does not seem to appear during winter in the IRI. T_e typically increase with increasing magnetic activity, especially at higher latitudes and at night. An obvious latitudinal variation of T_e is the decrease toward low latitudes during the night. It is most pronounced during summer, and is also present in spring and autumn. The T_e decrease does appear during winter nights, but is not as evident as in other seasons. Figure 4 shows T_e in autumn for 350 km. This feature may be ascribed to the latitudinal difference of the heat flow from the topside ionosphere [Schunk and Nagy, 2000].

5. Conclusion

Local and regional statistical models describing Millstone Hill IS radar observations of electron density, electron temperature and ion temperature have been developed using a bin-fit technique. The local models generate ionospheric variations with local time, day number, and altitude over 150-1000 km, as a function of the previous day's F107 and the Ap index for the previous 3 hours. F107 and Ap are keyed inputs to specify solar and geomagnetic activity. The regional models have a latitude coverage of 32-55° geodetic for 200-600 km altitude range. These climatology models are capable of reproducing primary ionospheric variation features seen in previous studies as well as several newly revealed features, such as the semiannual variation of electron density. They are accessible through the World Wide Web at the URL <http://www.openmadrigo.org>. The user can select model type (regional or local model) and parameter type (N_e , T_e , or T_i), and specify F107 and Ap

Figure 3

Figure 4

indices to get outputs in the form of various contour plots as well as ASCII data ready to be sent to the user's E-mail address. Several animated pictures demonstrating dynamic changes of ionospheric parameters are also available. We also provide portable software for recovery of model values.

Acknowledgments. We thank the members of the Haystack Observatory Atmospheric Sciences Group for assembling and maintaining the Madrigal Database of Millstone Hill incoherent scatter radar observations, which were the basis of this study. This research was supported by NSF Space Weather Grant ATM-9819413. The Millstone Hill incoherent scatter radar is supported by a cooperative agreement between the National Science Foundation and the Massachusetts Institute of Technology.

References

- Balan, N., G. J. Bailey, B. Jenkins, P. B. Rao, and R. J. Moffett, Variations of ionospheric ionization and related solar fluxes during an intense solar cycle, *J. Geophys. Res.*, *99*, 2243-2253, 1994.
- Balan, N., Y. Otsuka, S. Fukao, and G. J. Bailey, Equinoctial asymmetries in the ionosphere and thermosphere observed by the MU radar, *J. Geophys. Res.*, *103*, 9481-9486, 1998.
- Bilitza D., International Reference Ionosphere 2000, *Radio Sci.*, *36*, 261-275, 2001.
- Bilitza, D., and W. R. Hoegy, Solar activity variations of ionospheric plasma temperatures *Adv. Space Res.*, *10*, (8)81-90, 1990.
- Carlson, H. C., and G. M. Weill, Ionospheric heating by magnetic conjugate point photoelectrons, *J. Geophys. Res.*, *71*, 195-199, 1966.
- Evans, J. V., Cause of the mid-latitude evening increase in f_oF_2 , *J. Geophys. Res.*, *70*, 1175-1185, 1965.
- Evans, J. V., Seasonal and sunspot cycle variation of F region electron temperatures and protonospheric heat flux, *J. Geophys. Res.*, *78*, 2344-2349, 1973.
- Evans, J. V., J. M. Holt, W. L. Oliver, and R. H. Wand, On the formation of daytime troughs in the F-region within the plasmasphere, *Geophys. Res. Lett.*, *10*, 405-408, 1983.
- Foster, J. C., Storm-time plasma transport at middle and high Latitudes, *J. Geophys. Res.*, *98*, 1675-1689, 1993.
- Gentleman, W. V., Least squares computations by Givens transformations without square roots, *J. Inst. Math. Applics.*, *12*, 325-336, 1973.
- Holt, J. M., J. V. Evans, and R. H. Wand, Millstone Hill studies of the trough: boundary between the plasmapause and magnetosphere or not?, *Radio Sci.*, *18*, 947, 1983.
- Kohl, H. and J. W. King, Atmospheric winds between 100 and 700 km and their effects on the ionosphere, *J. Atmos. Terr. Phys.*, *29*, 1045-1062, 1967.
- Rodger, A. S., R.J. Moffett, and S. Quegan, The role of ion drift in the formation of ionisation troughs in the mid- and high-latitude ionosphere-a review, *J. Atmos. Terr. Phys.*, *54*, 1-30, 1992.
- Schunk, R. W., and A. F. Nagy, *Ionospheres - Physics, plasma physics, and chemistry*, Cambridge University Press,

- 340 pp., Cambridge, U. K., 2000.
- Rishbeth, H., How the thermospheric circulation affects the ionospheric F2-layer, *J. Atmos. Sol. Terr. Phys.*, *60*, 1385-1402, 1998.
- Rishbeth, H., C. F. Muller-Wodarg, L. Zou, T. J. Fuller-Rowell, G. H. Millward, R. J. Moffett, D. W. Idenden, and A. D. Aylward, Annual and semiannual variations in the ionospheric F2-layer, II, Physical discussion, *Ann. Geophys.*, *18*, 945-956, 2000.
- Rishbeth, H., and C. S. G. K. Setty, The F-layer at sunrise, *J. Atmos. Terr. Phys.*, *20*, 263-276, 1961.
- Vo, H. B. and J. C. Foster, A quantitative study of ionospheric density gradients at midlatitudes, *J. Geophys. Res.*, *106*, 21,555-21,563, 2001

J. M. Holt, S.-R. Zhang, and M. J. Buonsanto, Haystack Observatory, Massachusetts Institute of Technology, Route 40, Westford, MA 01886. (jmh@haystack.mit.edu, shumrong@haystack.mit.edu)

(Received _____)

¹Deceased October 20, 1999.

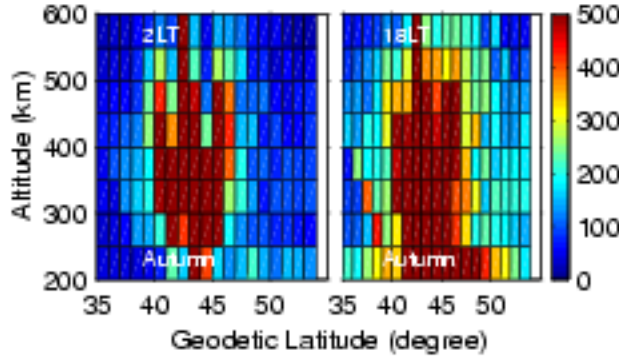


Figure 1. Distribution of number of data points with geodetic latitude and altitude for the regional models. The cell color represents the data number for the lower-left corner grid.

Figure 1. Distribution of number of data points with geodetic latitude and altitude for the regional models. The cell color represents the data number for the lower-left corner grid.

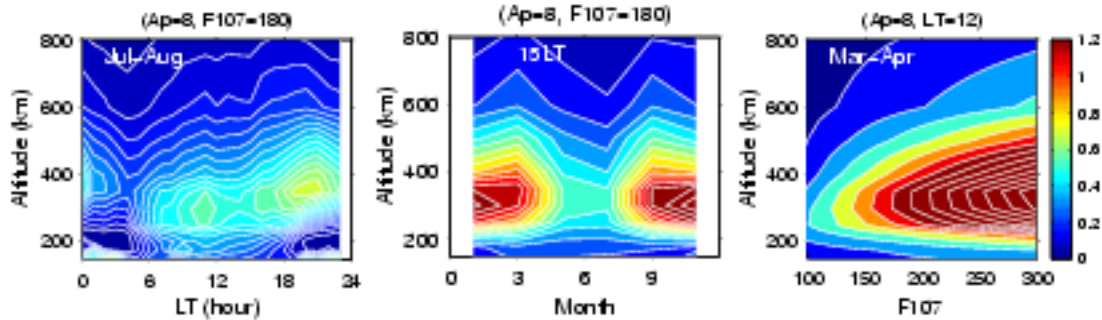


Figure 2. Iso-density contours with local time and altitude in summer (left panel), with month and altitude (middle panel), and with F107 and altitude (right panel) computed with the local electron density model for $A_p=8$. Electron density is in units of 10^{12} m^{-3} .

Figure 2. Iso-density contours with local time and altitude in summer (left panel), with month and altitude (middle panel), and with F107 and altitude (right panel) computed with the local electron density model for $A_p=8$. Electron density is in units of 10^{12} m^{-3} .

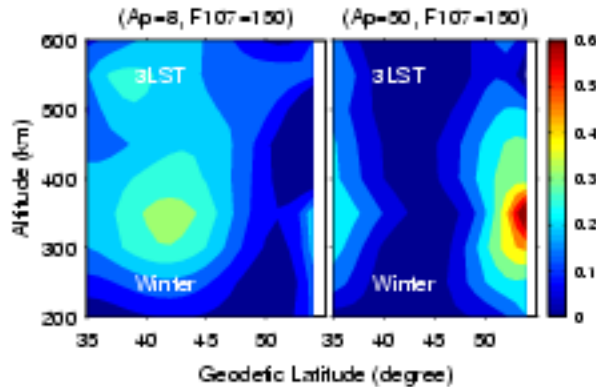


Figure 3. Subauroral ionospheric trough at 0300 LT in winter given by the regional electron density model for F107=150 and Ap=8 (left) and Ap=50 (right). Electron density is in units of 10^{12} m^{-3} .

Figure 3. Subauroral ionospheric trough at 0300 LT in winter given by the regional electron density model for F107=150 and Ap=8 (left) and Ap=50 (right). Electron density is in units of 10^{12} m^{-3} .

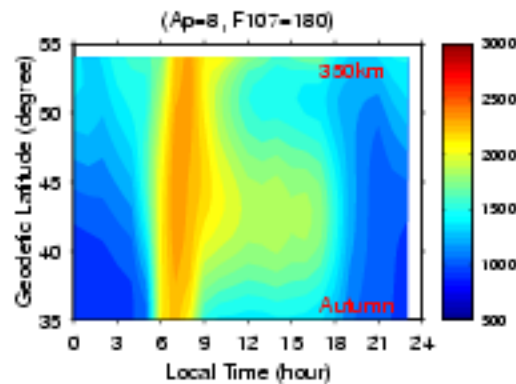


Figure 4. Electron temperature contours with geodetic latitude and local time for altitude 350 km in autumn with F107=180 and Ap=8.

Figure 4. Electron temperature contours with geodetic latitude and local time for altitude 350 km in autumn with F107=180 and Ap=8.

HOLT ET AL.: MILLSTONE HILL INCOHERENT SCATTER RADAR MODELS

HOLT ET AL.: MILLSTONE HILL INCOHERENT SCATTER RADAR MODELS

HOLT ET AL.: MILLSTONE HILL INCOHERENT SCATTER RADAR MODELS

HOLT ET AL.: MILLSTONE HILL INCOHERENT SCATTER RADAR MODELS

HOLT ET AL.: MILLSTONE HILL INCOHERENT SCATTER RADAR MODELS

HOLT ET AL.: MILLSTONE HILL INCOHERENT SCATTER RADAR MODELS

HOLT ET AL.: MILLSTONE HILL INCOHERENT SCATTER RADAR MODELS

HOLT ET AL.: MILLSTONE HILL INCOHERENT SCATTER RADAR MODELS

HOLT ET AL.: MILLSTONE HILL INCOHERENT SCATTER RADAR MODELS

HOLT ET AL.: MILLSTONE HILL INCOHERENT SCATTER RADAR MODELS

HOLT ET AL.: MILLSTONE HILL INCOHERENT SCATTER RADAR MODELS

HOLT ET AL.: MILLSTONE HILL INCOHERENT SCATTER RADAR MODELS

HOLT ET AL.: MILLSTONE HILL INCOHERENT SCATTER RADAR MODELS

HOLT ET AL.: MILLSTONE HILL INCOHERENT SCATTER RADAR MODELS

HOLT ET AL.: MILLSTONE HILL INCOHERENT SCATTER RADAR MODELS

HOLT ET AL.: MILLSTONE HILL INCOHERENT SCATTER RADAR MODELS

HOLT ET AL.: MILLSTONE HILL INCOHERENT SCATTER RADAR MODELS

HOLT ET AL.: MILLSTONE HILL INCOHERENT SCATTER RADAR MODELS